Temperature dependence of third-order elastic constants of potassium manganese fluoride

Wenwu Cao and Gerhard R. Barsch
Materials Research Laboratory and Department of Physics, The Pennsylvania State University, University Park, Pennsylvania 16802

Wenhua Jiang* and Mack A. Breazeale†
Department of Physics and Astronomy, The University of Tennessee, Knoxville, Tennessee 37996
(Received 22 June 1988)

The nonlinearity parameters along the three principal symmetry directions have been measured for $KMnF_3$ from 298 to 350 K by means of acoustic second-harmonic generation. In conjunction with our earlier data on the temperature dependence of the pressure derivatives of the elastic constants, the complete set of the six third-order elastic (TOE) constants has been determined in this temperature range. For c_{111}, c_{123}, and c_{166} the temperature dependence is linear, suggesting that the effect of the improper ferroelastic transition at 186 K is no longer present above 300 K. This permits us to eliminate the effects of zero-point and thermal motion and of the structural phase transition by linear extrapolation of the data to absolute zero temperature. The *bare* TOE constants thus obtained differ significantly from the room-temperature values. The *bare* (and the room-temperature) values exhibit large deviations from the Cauchy relations, indicating significant contributions from many-body forces.

I. INTRODUCTION

Of all ternary compounds with composition ABX_3 those occurring in the perovskite structure "are probably the most numerous, the most widely studied and the most important" (Ref. 1). However, many questions still remain to be answered, and the understanding of many material properties is still at the empirical level, especially for nonlinear phenomena. The fast development of technology in recent years, including the application of nonlinear properties,[2] demands better theoretical understanding of this important class of materials.

Since the commonly defined macroscopic nonlinearities result from the anharmonic nature of the interatomic forces, it is possible to correlate different nonlinearity parameters of the same order on the basis of a microscopic theory. For example, Achar *et al.*[3] used an anharmonic shell model to calculate the electrostriction constants of $SrTiO_3$ from the third-order elastic (TOE) constants. In lattice dynamical modeling the temperature variation can be taken into account either by explicitly including thermal lattice vibrations, or by eliminating thermal effects from the empirical data by extrapolating them to absolute zero temperature. The latter method would seem more reliable, especially in the presence of phase transitions. Since their effect can be manifest because of transformation precursors up to tens of degrees above the transition temperature T_c, the experimental data used for the extrapolation must extend to sufficiently high temperatures. The previous application of the anharmonic shell model based on this approach to evaluate the nonlinearity parameters of $SrTiO_3$ was not totally successful.[3] As this is possibly due to the large polarizability of the oxygen ions, it was considered desirable to measure the TOE constants of a perovskite which contains no oxygen and test the anharmonic shell model again.

Previously, two of the authors have studied the variation of the elastic constants of $KMnF_3$ as a function of both temperature and pressure,[4] from which three linear combinations of the six TOE constants have been determined. As the $KMnF_3$ crystal is extremely fragile, we have determined the remaining TOE constants by means of acoustic second-harmonic generation (SHG).[5] It is the purpose of the present paper to report results for the complete set of TOE constants and their temperature dependence. The extrapolated data can be used to check the applicability of the anharmonic shell model for this fluoride perovskite. According to the earlier work[4] the effect of the phase transition has subsided above room temperature, i.e., more than 100 K above the transition temperature (186 K). Therefore, in the present investigation the temperature is limited to the range from 290 to 350 K. In Sec. II we briefly describe the principle of the SHG technique and give experimental details. Section III contains the experimental results. Section IV deals with the discussion of our results and their comparison with data for other perovskites.

II. EXPERIMENTAL DETAILS

A. Sample

The two samples used in the present work were cut from a single crystal boule bought from Cristal Tec, Grennoble, France. One of them has oriented faces (110), $(1\bar{1}0)$, and (001) with the spacing between parallel faces of 1.0688, 1.0394, and 1.0630 cm, respectively. This sample was used also for the previous hydrostatic pressure work.[4] The other one contains one pair of polished (111) faces with 0.7559-cm interfacial distance. Gold coating

about 1000 Å thick was vapor deposited onto the polished surfaces by using a small conventional vacuum evaporator.

B. Wave propagation in a nonlinear medium

If a plane wave propagates through a nonlinear medium, the wave profile is distorted and the frequency spectrum contains higher-order harmonics. The nonlinearity also causes coupling between different acoustic modes through the equations of motion. Goldberg[6] proved that pure transverse vibration modes do not exist for a nonlinear system. However, for a cubic crystal pure longitudinal modes still exist in [100], [110], and [111] if only up to the third-order terms are kept in the elastic energy expansion. Taking the x coordinate along one of these three symmetry directions, the x component of the equation of motion for a longitudinal displacement field $\mathbf{u}(\mathbf{x})$ has the following form:[7,8]

$$\rho_0 \ddot{u}_x = K_2(u_{x,xx} + 3u_{x,x}u_{x,xx}) + K_3 u_{x,x}u_{x,xx} \ . \quad (2.1)$$

Here ρ_0 denotes the density of the crystal. K_2 and K_3 are linear combinations of second- and third-order elastic constants, respectively, and are shown in Table I for the three cubic point groups O_h, O, and T_d. The subscripts after the comma indicate the spatial derivatives with respect to those variables. If the wave amplitude is small Eq. (2.1) can be solved by perturbation; the approximate solution after one iteration is[5,7]

$$u_x = A_1 \sin(kx - \omega t) - A_2 \cos[2(kx - \omega t)] \ , \quad (2.2)$$

where ω is the angular frequency and k is the wave number. The generated second harmonic has an amplitude A_2 given by

$$A_2 = (A_1^2 k^2 \beta x)/8 \ , \quad (2.3)$$

where x is the distance traveled by the elastic wave. The nonlinearity parameter β is defined as the negative ratio of the coefficients of the nonlinear term and the linear term in the equation of motion. For pure longitudinal wave propagation in the high-symmetry directions of a cubic system, β can be written as

$$\beta = -(3K_2 + K_3)/K_2 \ , \quad (2.4)$$

and can be determined from the ratio of the amplitudes A_1 and A_2 by means of Eq. (2.3).

C. Apparatus

The apparatus used for the present work was developed by Gauster and Breazeale.[9] The basic idea is as follows. An initially sinusoidal ultrasonic wave is sent from one end into a sample which serves as a nonlinear medium. As the wave arrives at the opposite surface it is distorted by the nonlinearity; in other words, the surface vibration at the other end contains the frequencies of the driving wave and of the generated higher harmonics. If this free end is used to form a parallel-plate capacitor with another fixed electrode, the mechanical vibrations of different frequency can be transformed into electrical signals with the help of a dc bias voltage across the capacitor. Through a delicate calibration procedure (see below), the nonlinearity parameter β defined by Eq. (2.3) can be determined and gives the desired information about the TOE constants. The apparatus consists of standard ultrasonic pulse equipment, with the addition of rf amplifiers tuned to the 30 MHz fundamental and the 60 MHz second harmonic, each having a bandwidth of 10 MHz. The most important part of the apparatus is the receiver capacitor shown in Fig. 1 which is formed by one of the sample faces and the detector button. The spacing of the capacitor can be adjusted through either polishing the button surface or the ground ring on which the sample rests. In the present work, a detector button with diameter of 5.095 mm is used and the spacing is adjusted to 10-12 μm to give a capacitance of 14–16 pF. A bias voltage of 160 V is applied to the capacitor. A 30-MHz X-cut quartz transducer is bonded to the top surface of the sample by a special glue peeled from a Scotch tape (No. 845, 3M company, Minnesota). The electrical pulses are applied to the transducer from the top connector and generate a longitudinal acoustic wave through the transducer. The wave causes the bottom surface of the sample to vibrate and induces an ac voltage between the two leads of the capacitor. From the capacitor signal the magnitudes of the fundamental and second-harmonic waves can be determined with the experimental arrangement shown in Fig. 2.

Because $KMnF_3$ is very brittle, the three supporting rods of the original design were replaced by fine screw (10–64) rods with three more hand-adjustable nuts to support the weight of the top electrode. The original design was made for room temperature and below; therefore, in order to extend the temperature region, a furnace with a 5-in. inner diameter was built so as to contain the whole assembly for uniform heating.

TABLE I. The quantities K_2 and K_3 for longitudinal wave propagation along the pure mode directions for the cubic point groups O_h, O, and T_d [from Green (Ref. 8)].

Direction of wave propagation	K_2	K_3
[100]	c_{11}	c_{111}
[110]	$\frac{1}{2}(c_{11}+c_{12}+2c_{44})$	$\frac{1}{4}(c_{111}+3c_{112}+12c_{166})$
[111]	$\frac{1}{3}(c_{11}+c_{12}+4c_{44})$	$\frac{1}{9}(c_{111}+6c_{112}+12c_{144}+24c_{166}+2c_{123}+16c_{456})$

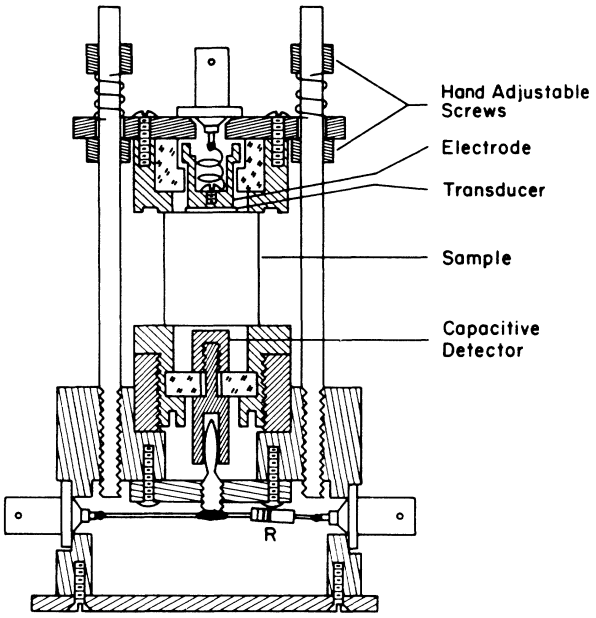

FIG. 1. Schematic diagram of the capacitance detector [after Breazeale and Philip (Ref. 5)].

D. Calibration procedure

The signal from the detector is fed to either a 30- or a 60-MHz bandpass amplifier, and a boxcar integrator is used to measure the output from these amplifiers (Fig. 2). In order to detect the amplitudes of the fundamental and second-harmonic waves received by the capacitive detector, a comparison method is used. The equivalent circuit is shown in Fig. 3. After recording the output from the amplifiers by the boxcar integrator, the acoustic signal is turned off, i.e., switch S_1 in Fig. 3 is open. Next, a substitutional signal is introduced in the place of the acoustic signal, i.e., S_2 of Fig. 3 is closed. The amplification of the amplifier is kept the same for acoustic and substitutional signals. By adjusting the amplitude of the substitutional signal one can get the same reading in the boxcar integrator for both signals. Therefore, by measuring the substitutional signal, which is the same as that generated by the capacitance detector, the amplitude of the acoustic wave can be calculated.

The argument is as follows. If a sinusoidal wave with amplitude A is propagating in a sample, the vibration in the stress-free surface will have an amplitude of $2A$ because of reflection. Consequently, the gap spacing of the detector will change according to

$$S = S_0 + 2A \sin(\omega t) . \tag{2.5}$$

The capacitance of the detector is approximately given by[5]

$$1/C = (1/C_0)[1 + (2A/S_0)\sin(\omega t)] , \tag{2.6}$$

where C_0 is the static capacitance of the receiver,

$$C_0 = (\epsilon\alpha/S_0) . \tag{2.7}$$

α is the area of the detector button, ϵ is the dielectric constant, and S_0 is the static gap spacing. It can be shown that the generated voltage V (magnitude) across the detector can be written as

$$V = 2AV_b/S_0 , \tag{2.8}$$

where V_b is the bias dc voltage applied to the detector. As shown in Fig. 3, if i_D represents the effective current from the detector, then we have

$$i_D = \sqrt{2}AV_b\omega C_D/S_0 . \tag{2.9}$$

where ω is the angular frequency of the acoustic wave and C_D is the capacitance of the detector. Therefore, if i_D can be measured, the amplitude A is obtained from

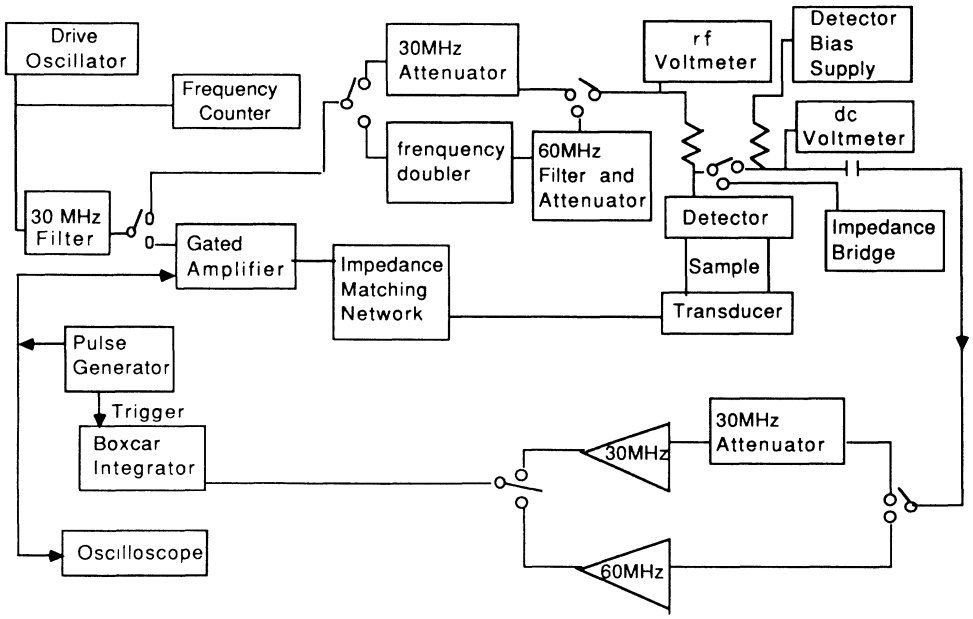

FIG. 2. Block diagram of the electronic circuit for the second-harmonic generation measurement.

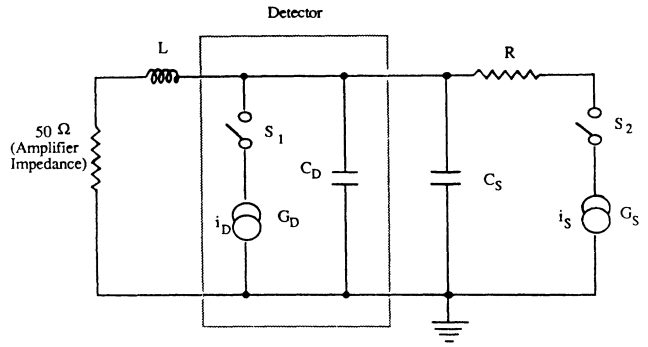

FIG. 3. Equivalent circuit of the comparison method for absolute amplitude measurement (Ref. 5).

Eq. (2.9).

The measurement of the substitutional current is achieved by measuring the voltage V_S across a 10-kΩ resistor. For high frequency, the impedance of the resistor contains both real and imaginary parts. In addition, the stray capacitance and wire inductance will also contribute to the circuit impedance. Therefore the total impedance is measured by a vector meter as a function of frequency. Near 30 MHz, the total impedance magnitude is given by

$$|Z_1| = (13.5525 - 0.413\,08\times10^{-7} f)\ \text{k}\Omega\ . \quad (2.10a)$$

Near 60 MHz, the function may be written as

$$|Z_2| = (13.707\,16 - 0.513\,38\times10^{-7} f)\ \text{k}\Omega \quad (2.10b)$$

where, the input frequency f is in units of Hz. Even though the substitutional current is small, the voltage V_S across the resistor is still measurable since the impedance is very large. V_S is recorded by a broadband sampling voltmeter.

If the condition $i_D = i_S$ is satisfied, from Eq. (2.7) and (2.9) we finally derive the amplitude of the ultrasonic wave as

$$A = \frac{\epsilon d^2 V_S}{8\sqrt{2} V_b f C_D^2 |Z|}\ . \quad (2.11)$$

where d is the diameter of the detector button and we have used the relation $i_S = V_S/|Z|$.

E. Diffraction correction

Equation (2.3) for the relation between the amplitudes A_1, A_2, and the nonlinearity parameter β is based on the assumption that the fundamental and the second-harmonic wave propagate as plane waves in an infinite medium. Under actual experimental conditions diffraction effects due to the finite size of the transducer arise. Denoting the actual (uncorrected) and the equivalent plane wave (corrected) amplitude of the received signal by A_u and A_c, respectively, a correction factor can be defined by

$$D = A_u / A_c \quad (2.12)$$

and is given by the Lommel diffraction integral.[10] Denoting the radii of the circular source and receiver by R_s and R_r, respectively, and assuming $R_s = R_r = R$, it is for $(kR)^{1/2} \gg 1$ (Ref. 10)

$$D = \{[\cos\xi - J_0(\xi)]^2 + [\sin\xi - J_1(\xi)]^2\}^{1/2}\ . \quad (2.13)$$

Here $\xi = 2\pi/s$, where $s = 2\pi L/kR^2$, L is the distance between source and receiver, k the wave number, and J_0 and J_1 the Bessel functions of zeroth and first order, respectively. The function $D(s)$ shows oscillatory behavior superimposed on an overall decrease with increasing s (Ref. 11); for $s = 0$ it is $D(0) = 1$.

In order to test Eqs. (2.12) and (2.13) Blackburn and Breazeale[12] performed SHG measurements on Cu single crystals as a function of R and found, somewhat surprisingly, that the nonlinearity parameter β as calculated from Eq. (2.3) becomes approximately constant (independent of s) if only the amplitude A_1 of the fundamental, but not that of the second harmonic (A_2) is corrected according to (2.12) and (2.13). Since the second harmonic is not generated at the transducer, but rather produced along the path of the ultrasonic beam, this could be taken as an indication that the correction for A_2 is negligibly small. Alternatively, however, the observed near-constancy of β could also arise from a cancellation with other effects that depend on the parameter s, such as the electric stray field around the circumference of the receiver button and/or deviations of the crystal-receiver-button configuration from that of an ideal plane-parallel capacitor. If the diffraction correction for A_2 were included the total correction for β would become smaller.[13] Other approximations implicit in Eq. (2.13) are, first, the assumption that the oscillations of the transducer can be described by an oscillatory motion of a rigid piston, and second, that the longitudinal elastic wave generated propagates in a fluid, i.e., in an isotropic medium with zero shear resistance. Furthermore, the assumption $R_s = R_r$ will not be valid in general.[14] While keeping in mind these limitations and uncertainties we will below follow the above procedure[11,12] for applying the diffraction correction to our present data.

III. EXPERIMENTAL RESULTS

A. Nonlinearity parameters and TOE constants at room temperature

Since the amplitude of the second-harmonic wave is very small ($\sim 10^{-13}$ m), the signal generated by the second harmonic is also very small (< 1 mV). In measuring such a small signal for high frequency, the environmental noise and the electronic system noise affects the measured results. According to Eq. (2.3) A_2 is proportional to A_1^2 for a given frequency. If the noise contribution can be considered as constant, the measured value of A_2 contains the actual signal and the noise, i.e.,

$$A_2 = (A_1^2 k^2 L\beta)/8 + C_{\text{noise}}\ , \quad (3.1)$$

where L is the sample length. (The effect of the noise on A_1 is negligible since A_1 is more than 1000 times larger than the noise level.) In calculating the nonlinearity pa-

rameter β from Eq. (2.3), the noise contributions can be eliminated by means of Eq. (3.1). The results of A_2 versus A_1^2 in the three symmetry directions are shown in Fig. 4 together with straight lines obtained from least-squares fitting. It is apparent that the linear relations between A_2 and A_1^2 are well satisfied in these directions, but that the intercepts of the curves with the vertical axis and therefore the noise levels are different. This is corrected by using Eq. (3.1). From the slopes in Fig. 4 the nonlinearity parameters β and K_3 can be calculated; the results obtained without and with the diffraction correction are listed in Table II.

Since the diffraction correction for different radii of the source and the receiver is not known[14] we have taken the radius R entering Eq. (2.13) as that of the transducer (0.325 cm). By using instead the radius for the receiver (0.25 cm) the correction becomes larger and the magnitude of the corrected values of K_3 about 2–3 % smaller.

From hydrostatic pressure measurements the partial contractions of the TOE constants can be obtained, viz., for cubic symmetry,[4]

$$\begin{aligned}\gamma_{11}^{(3)}&=c_{111}+2c_{112}\ ,\\ \gamma_{12}^{(3)}&=2c_{112}+c_{123}\ ,\\ \gamma_{44}^{(3)}&=c_{144}+2c_{166}\ .\end{aligned}\tag{3.2}$$

From these equations and from the expressions for K_3 in Table I the six independent TOE constants for cubic (O_h, O, and T_d) symmetry can be calculated according to

$$\begin{aligned}c_{111}&=K_3^{[100]}\ ,\\ c_{112}&=-\tfrac{1}{2}K_3^{[100]}+\tfrac{1}{2}\gamma_{11}^{(3)}\ ,\\ c_{166}&=\tfrac{1}{24}K_3^{[100]}+\tfrac{1}{3}K_3^{[110]}-\tfrac{1}{8}\gamma_{11}^{(3)}\ ,\\ c_{123}&=K_3^{[100]}-\gamma_{11}^{(3)}+\gamma_{12}^{(3)}\ ,\\ c_{144}&=-\tfrac{1}{12}K_3^{[100]}-\tfrac{2}{3}K_3^{[110]}+\tfrac{1}{4}\gamma_{11}^{(3)}+\gamma_{44}^{(3)}\ ,\\ c_{456}&=\tfrac{9}{16}K_3^{[111]}-\tfrac{1}{16}\gamma_{11}^{(3)}-\tfrac{1}{8}\gamma_{12}^{(3)}-\tfrac{3}{4}\gamma_{44}^{(3)}\ .\end{aligned}\tag{3.3}$$

Combined with the data from hydrostatic pressure measurements,[4] the six TOE constants of $KMnF_3$ have been calculated at room temperature. The results obtained without and with the diffraction correction are given in Table III. It is apparent that for some of the TOE constants, notably so for c_{112}, c_{144}, and c_{456}, the diffraction correction is larger than the values themselves. This is due to the circumstance that the sums of the nonlinearity parameters K_3 in Eqs. (3.3b), (3.3d), and (3.3f) have approximately the same magnitude, but the opposite sign than the corresponding sums of $\gamma_{\mu\nu}^{(3)}$ from the hydrostatic pressure data; thus a small change in K_3 causes a large change in the TOE constants.

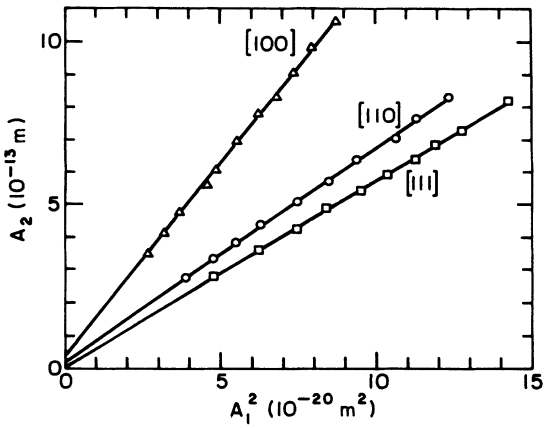

FIG. 4. Relation between A_2 and A_1^2 at room temperature for principal symmetry directions. A_1 and A_2 are the amplitudes of the fundamental and of the second-harmonic waves, respectively.

B. Temperature dependence of K_3

In order to measure the temperature dependence of the nonlinearity parameters, the apparatus shown in Fig. 1 was put into an electrically heated furnace whose temperature is controlled by a precision adjustable voltage transformer. Because of the relatively small diameter of the furnace (5 in.) and the requirement of thermal equilibrium, the calibration is done by a relative method. The basic idea of the relative method is as follows: If the value of β is known at a particular temperature T_1, and if the ratio of $\beta(T_2)/\beta(T_1)$ can be measured, then the entire temperature dependence can be determined.

TABLE II. Slopes of linear plots of Fig. 4; uncorrected and corrected room-temperature values of the nonlinearity parameters β and K_3, uncorrected and corrected bare values K_3^0, plus high-temperature limit of uncorrected and corrected temperature coefficients $\kappa_3=(\partial K_3/\partial T)_p$. In all cases the first entry represents the uncorrected value (without diffraction correction), and the second entry (in parentheses) the corrected value.

Propagation direction	$\partial A_2/\partial(A_1)^2$ (10^7 m^{-1})	β	K_3 (10^{10} N/m^2)	K_3^0 (10^{10} N/m^2)	κ_3 (10^8 N/m^2 K)
[100]	1.191	8.90	−136.7	−130.6	−2.50
		(7.22)	(−117.4)	(−122.3)	(−2.07)
[110]	0.657	4.50	−78.1	−53.5	−9.72
		(3.65)	(−69.3)	(−44.1)	(−9.44)
[111]	0.572	4.65	−66.1	−105.9	11.39
		(3.96)	(−60.9)	(−95.6)	(9.99)

TABLE III. Room-temperature values $c_{\mu\nu\lambda}$ and *bare* values $c^0_{\mu\nu\lambda}$ of TOE constants (in 10^{10} N/m^2), and high-temperature limit of temperature coefficients $D_{\mu\nu\lambda}=\partial c_{\mu\nu\lambda}/\partial T$ (in 10^8 N/m^2) of adiabatic TOE constants. In all cases the first entry represents the uncorrected value (without diffraction correction) and the second entry (in parentheses) the corrected value.

$\mu\nu\lambda$	111	112	166	123	144	456
$c_{\mu\nu\lambda}$	−136.7	−2.5	−14.0	−44.0	1.8	−2.5
	±3.0	±2.1	±1.7	±5.2	±3.6	±2.9
	(−117.4)	(−12.2)	(−10.3)	(−24.7)	(−5.7)	(0.4)
$c^0_{\mu\nu\lambda}$	−130.6	−17.5	−2.6	−5.1	−22.0	−23.8
	±3.1	±2.2	±2.3	±6.3	±4.6	±4.9
	(−122.3)	(−21.7)	(0.9)	(3.3)	(−28.9)	(−18.0)
$D_{\mu\nu\lambda}$	−2.50	3.03	−3.79	4.7	7.5	4.9
	±0.25	±0.22	±0.50	±1.2	±1.0	±1.3
	(−2.07)	(2.82)	(−3.68)	(5.1)	(7.3)	(4.1)

From Eqs. (2.7) and (2.8) the magnitudes of the fundamental- and second-harmonic waves can be written as

$$A_i=\epsilon\alpha V_i/2V_bC_D, \quad (i=1,2) \tag{3.4}$$

where V_i is the voltage across the capacitance detector generated by the corresponding acoustic wave with amplitude A_i. According to Eq. (2.3) the ratio of β at different temperatures can be written as

$$\frac{\beta(T_2)}{\beta(T_1)}=\frac{A_2(T_2)A_1^2(T_1)v^2(T_2)L(T_1)}{A_2(T_1)A_1^2(T_2)v^2(T_1)L(T_2)} , \tag{3.5}$$

where we have used the relation between wave vector k and velocity v, i.e., $k=2\pi f/v$, and $L(T)$ is the sample length at temperature T.

When the temperature is changed, for the same bias voltage V_b and the same amplification of the amplifiers, the acoustic input energy will be adjusted first to give the same V_1, i.e., $V_1(T_1)=V_1(T_2)$. From Eq. (3.4) we have

$$\frac{A_1^2(T_1)}{A_1^2(T_2)}=\frac{C_D^2(T_2)}{C_D^2(T_1)} . \tag{3.6}$$

Next, the bias voltage V_b is adjusted to make V_2 the same for different temperatures. Then we obtain from Eq. (3.4)

$$\frac{A_2(T_2)}{A_2(T_1)}=\frac{C_D(T_1)V_b(T_1)}{C_D(T_2)V_b(T_2)} . \tag{3.7}$$

The velocity square term is related to K_2 through the relation $\rho v^2=K_2$. In the temperature region covered in our experiments, the thermal expansion coefficient $\alpha_{\rm th}$ can be considered as temperature independent,[15] so that ρ and L at different temperatures are related by

$$L(T_2)=L(T_1)[1+\alpha_{\rm th}(T_2-T_1)] , \tag{3.8}$$

$$\rho(T_2)=\rho(T_1)[1-3\alpha_{\rm th}(T_2-T_1)] . \tag{3.9}$$

Upon substituting Eqs. (3.6)–(3.9) into Eq. (3.5) one obtains

$$\frac{\beta(T_2)}{\beta(T_1)}=\frac{C_D(T_2)V_b(T_1)K_2(T_2)}{C_D(T_1)V_b(T_2)K_2(T_1)[1-3\alpha_{\rm th}(T_2-T_1)][1+\alpha_{\rm th}(T_2-T_1)]} . \tag{3.10}$$

Since the room temperature value of β has been measured and K_2 is known, only the changes of C_D and V_b versus temperature are needed. It should be noted that the noise contribution for A_2 is included in this method and will introduce an additional error of about 1%.

With the aid of Eq. (3.10), the nonlinearity parameter β was measured as a function of temperature in the three symmetry directions. These values are used to calculate the parameter K_3 through Eq. (2.3), and the results are shown in Fig. 5. $K_3^{[100]}$ is equal to the third-order elastic constants c_{111} and shows only weak temperature dependence [1.8% change over the investigated temperature range] with negative slope. $K_3^{[110]}$ decreases with temperature in a nearly linear manner for temperatures above 320 K, but the change is much larger near room temperature, possibly because of some remaining effect of the phase transition. The data for $K_3^{[111]}$ show relatively larger scatter, and a minimum occurs at about 313 K. This behavior was confirmed by repeating the measurements three times and taking data both during heating and cooling. There are several possible reasons for this behavior.

(i) Effect of the phase transition. From the hydrostatic pressure measurements at low temperature[4] it is apparent that the effect of the phase transition persists even up to room temperature and affects some quantities more than others. It is conceivable that one particular third-order elastic constant is responsible for this behavior.

(ii) Competing effects. $K_3^{[111]}$ contains the contributions from all six TOE constants. Some of these con-

stants increase with temperature and others decrease with temperature. The minimum could occur where these two effects cancel.

(iii) Sample defects. As sample 2 was not cut from the best part of the original crystal boule, it could contain defects and internal strain. In this case the unusual behavior shown in Fig. 5 should occur only for this particular sample (sample 2). It should be noted, however, that modulations in the temperature dependence of $K_3^{[111]}$ similar to those in Fig. 5 were also observed[16] for $KZnF_3$, which does not undergo a structural phase transition. This suggests the possibility that this effect is due to a contribution from dislocation motion.[17] In order to clarify this matter, additional measurements on a different sample are required, with special attention to be given to SHG in [111].

For $KMnF_3$ the second-order elastic constants,[4] and the linear combinations of TOE constants obtained from the hydrostatic pressure dependence of the second-order elastic constants,[4] and for $SrTiO_3$ the TOE constants (Ref. 18) exhibit a cusp-like anomaly near the structural transition temperature [186 K for $KMnF_3$]. This anomaly has been attributed to fluctuations of the order parameter [the rotation angles of the MnF_6 octahedra] and should for $T > T_c$ decay as $(T-T_0)^{-\delta}$ (Refs. 19 and 20). For $KMnF_3$ the second-order elastic constants and the partial contractions of TOE constants approach a linear temperature dependence in the range from about 320 to 350 K (Ref. 4), in agreement with that obtained theoretically from first-order anharmonic perturbation theory[21–23] in the high-temperature limit $T > \Theta$ (Θ is the Debye temperature). Therefore, the data in Fig. 5 suggest that the effect of the phase transition has subsided above about 320 K also for the nonlinearity parameters K_3 and for the individual TOE constants. Thus we have fitted the temperature dependence of K_3, without and with the diffraction correction for all three directions from 320 to 350 K, to linear relations of the form

$$K_3 = K_3^0 + \kappa_3 T \ . \tag{3.11}$$

The static values K_3^0 represent the *bare* constants, without zero-point motion and thermal contributions, and without the contribution from the phase transition. Together with the temperature coefficients κ_3 they are also listed in Table II, both for the uncorrected and for the corrected data. It is apparent that the diffraction correction amounts to about 20% for $K_3^{[110]}$ and $\kappa_3^{[100]}$, and to about 10% for the remaining four quantities.

C. Temperature dependence of third-order elastic constants

Combining the experimental data under hydrostatic pressure[4] and the SHG measurements, the six TOE constants for $KMnF_3$ were calculated from Eq. (3.3) as functions of temperature. Since the diffraction correction is rather large and somewhat uncertain we have calculated these results in two different ways.

First, we show in Fig. 6 the uncorrected TOE constants versus temperature that were calculated at different temperatures from the measured data of $\gamma_{\mu\nu}^{(3)}$ and K_3 from Ref. 4 and Fig. 5, respectively. Because of the

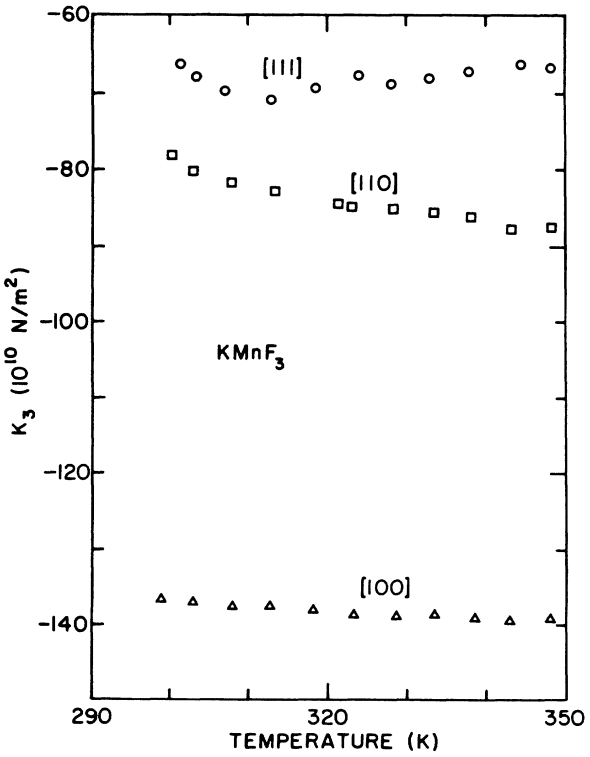

FIG. 5. Temperature dependence of the parameter K_3 (without diffraction correction) along the principal symmetry directions. Expressions for K_3 are listed in Table I.

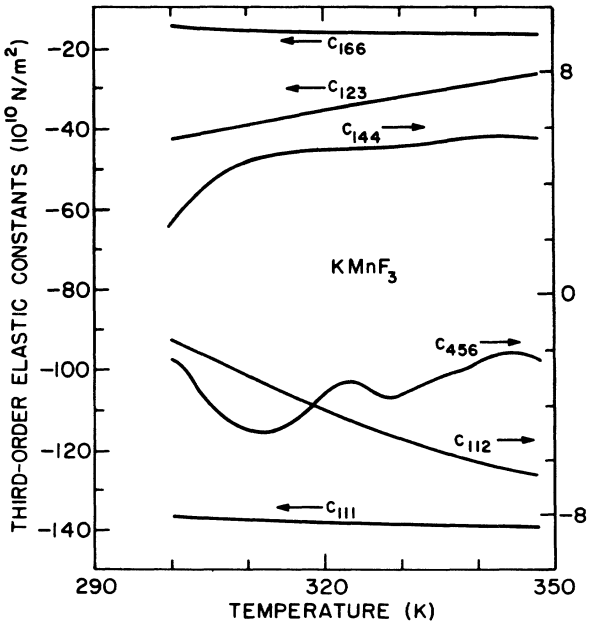

FIG. 6. Third-order elastic constants (without diffraction correction) vs temperature. Note greatly expanded scale of ordinate on rhs.

more limited temperature range accessible with the SHG equipment, these calculations were performed only for temperatures from 300 to 348 K. Except for $K_3^{[111]}$, which shows large scatter, the experimental data were refitted smoothly to polynomial curves (up to fourth order, as necessary) in this calculation. The following features are apparent from Fig. 6. c_{111} follows a fairly flat curve and decreases slowly with increasing temperature (only 1.8% change over the investigated temperature range), c_{112} and c_{166} decrease with increasing temperature; and c_{166} is approaching an asymptotic straight line in the high temperature region. c_{123} and c_{144} increase with temperature, and c_{144}, but not c_{123}, shows strong curvature; c_{456} shows unusual behavior, for the possible reasons discussed above. Except for c_{144}, c_{112}, and c_{456} above about 320 K the temperature dependence of the TOE constants is linear.

Second, we list in Table III the *bare* TOE constants and the high-temperature limits $D_{\mu\nu\lambda}$ of the temperature coefficients of the TOE constants as defined by

$$c_{\mu\nu\lambda}=c^0_{\mu\nu\lambda}+D_{\mu\nu\lambda}T\ . \tag{3.12}$$

Both $c^0_{\mu\nu\lambda}$ and $D_{\mu\nu\lambda}$ were calculated according to Eq. (3.3) from the corresponding *bare* quantities $\gamma^{(3),0}_{\mu\nu}$ and K^0_3, and from the high-temperature limits of the temperature coefficients $B_{\mu\nu}$ and κ_3 of the partial contractions $\gamma^{(3)}_{\mu\nu}$ of the (mixed adiabatic-isothermal) TOE constants and of the (adiabatic) nonlinearity parameters K_3 as given in Ref. 4 (Table I) and Table II above, respectively. For both $c^0_{\mu\nu\lambda}$ and $D_{\mu\nu\lambda}$ we list in Table III both the uncorrected and the corrected values. The basis for obtaining the error estimates included in Table III is explained below.

It is apparent that, with the exception of c_{144} and c_{456}, the difference $c^c_{\mu\nu\lambda}-c^u_{\mu\nu\lambda}$ between corrected (c) and uncorrected (u) values is noticeably smaller for the *bare* quantities than for the room-temperature values. Furthermore, it can be seen that the diffraction correction affects the TOE constants $c_{\mu\nu\lambda}$ and $c^0_{\mu\nu\lambda}$ more strongly, but that its effect on the temperature coefficients is confined to about 10–20% only. Consequently, the necessary modification of Fig. 6 resulting from the diffraction correction would consist mostly of vertical shifts of the curves for the TOE constants, but would have only little effect on their slopes. An exception occurs for c_{112} which would pass through a shallow minimum near 350 K that results from a corresponding minimum of $\gamma^{(3)}_{11}$ (Ref. 4, Fig. 4) so that the temperature coefficients in Fig. 6 and in Table III are of opposite sign.

We have included in Table III errors of the uncorrected data by *estimating* for the room temperature data of $\gamma^{(3)}_{11}$, $\gamma^{(3)}_{12}$, $\gamma^{(3)}_{44}$, $K_3^{[100]}$, $K_3^{[110]}$, and $K_3^{[111]}$ uncertainties of ± 3, 3, 1, 3, 5, 5 (in units of 10^{10} Nm^{-2}), respectively, and $\pm 10\%$ for the relative errors of the temperature derivatives of $\gamma^{(3)}_{11}$, $\gamma^{(3)}_{12}$, $\gamma^{(3)}_{44}$, $K_3^{[100]}$, $\pm 15\%$ for $K_3^{[110]}$, and $\pm 20\%$ for $K_3^{[111]}$. The errors of the room-temperature values and of the high-temperature limit of the temperature coefficients of the TOE constants were calculated from Eqs. (3.3) by means of Gauss's error-propagation law. The errors for the *bare* TOE constants $c^0_{\mu\nu\lambda}$ were calculated from the aforementioned errors on the basis of Eq. (3.12), again by using the error-propagation law. Since the diffraction correction is likely to be subject to systematic errors we refrain from including errors for the corrected data in Table III.

Finally, we note that for c_{111} the room-temperature value and the temperature coefficient listed in Table III and the data shown in Fig. 6 versus temperature are purely adiabatic quantities. However, since the other TOE constants were calculated according to Eq. (3.3) from the mixed adiabatic-isothermal partial contractions $\gamma^{(3)}_{\mu\nu}$ of Ref. 4 and from the adiabatic nonlinearity parameters K_3 of the present work the corresponding quantities are intermediate values. In principle it is, of course, possible to convert all quantities to purely isothermal or adiabatic conditions.[24] However, for $KMnF_3$ not all data required for this conversion are available. In Ref. 4 we have therefore restricted this conversion to the room-temperature data by calculating the specific heat and its temperature coefficient from the Debye expression and by using the elastic Debye temperature. Extension to higher temperature would introduce errors in the temperature coefficients of the $\gamma^{(3)}_{\mu\nu}$. Furthermore, experimental thermal-expansion data[15] are only available below 300 K, and their extrapolation to higher temperature introduces additional uncertainties. On the other hand, we believe that the *bare* values of the TOE constants in Tables III and IV are not affected by these uncertainties because both the measured mixed values of $\gamma^{(3)}_{\mu\nu}$ and the values converted to purely isothermal conditions exhibit linear temperature dependence in the high-temperature limit and extrapolate linearly to the same static values $\gamma^{(3),0}_{\mu\nu}$. This is consistent with the behavior expected from first-order anharmonic perturbation theory.[21–24]

D. Recommended values of *bare* TOE constants

The primary goal in measuring the TOE constants of $KMnF_3$ versus temperature was to determine their *bare*

TABLE IV. Comparison of "recommended" experimental *bare* second- and third-order elastic constants with averages of theoretical values from options (i) and (ii) (in 10^{10} N/m^2). Calculated Coulomb contributions are shown in parentheses.

	c_{11}	c_{12}	c_{44}	c_{111}	c_{112}	c_{166}	c_{123}	c_{144}	c_{456}
Extrap.	12.552	4.529	2.711	−124	−21	0.4	2	−28	−19
Expt.				±5	±5	±2	±13	±5	±5
Theor.	12.552	3.620	3.620	−103.8	−30.3	−30.3	−6.0	−6.0	−6.0
	(−12.64)	(1.578)	(1.578)	(65.1)	(−1.0)	(−1.0)	(−6.0)	(−6.0)	(−6.0)

values pertaining to the static crystal. However, as discussed in Sec. II E, the simplified diffraction correction most likely represents only an upper limit. Therefore we suggest to consider as the most probable values a set of revised data obtained from the following two plausible *assumptions.*

(i) The actual diffraction correction amounts only to 85% of the calculated diffraction correction.

(ii) The total error of the recommended final value is according to the Gauss error-propagation law composed of the error $\Delta c^{0,u}_{\mu\nu\lambda}$ of the uncorrected (u) *bare* TOE constants, and of the amount $0.15(c^{c}_{\mu\nu\lambda}-c^{u}_{\mu\nu\lambda})$ by which the calculated diffraction correction (c) has been reduced according to (i).

The "recommended" final *bare* values

$$c^{0,r}_{\mu\nu\lambda}=c^{0,u}_{\mu\nu\lambda}+0.85(c^{0,c}_{\mu\nu\lambda}-c^{0,u}_{\mu\nu\lambda})$$

and their total error

$$\Delta c^{0,r}_{\mu\nu\lambda}=\{(\Delta c^{0,u}_{\mu\nu\lambda})^2+[0.15(c^{0,c}_{\mu\nu\lambda}-c^{0,u}_{\mu\nu\lambda})]^2\}^{1/2}$$

as calculated from the values in Table III are listed in Table IV, together with the *bare* values of the second-order elastic constants from Ref. 4. In Sec. IV A they will be compared with theoretical results.

It should be noted that in all cases the partial contractions $\gamma^{(3),0}_{\mu\nu}$ calculated either from the uncorrected or from the corrected *bare* TOE constants in Table III, or from the "recommended" final values in Table IV are identical with the *bare* values reported in Ref. 4 (Table I).

IV. DISCUSSION

A. Deviations from Cauchy relations

The Cauchy relations for the second- and third-order elastic constants are, respectively,

$$c_{12}=c_{44}\ , \tag{4.1}$$

$$c_{112}=c_{166}\ , \tag{4.2a}$$

$$c_{123}=c_{144}=c_{456}\ . \tag{4.2b}$$

They are valid for a static (i.e., without zero-point and thermal motion) centrosymmetric crystal with central force-type interatomic forces only.

The corrected data in Table III, the recommended values in the first row of Table IV, and the room-temperature values of the second-order elastic constants of Ref. 4 show that *relatively* large deviations occur for Eqs. (4.1) and the second of the two equations (4.2b), both at room temperature and for the *bare* values; and that the room-temperature data show relatively small (large) deviations for Eq. (4.2a) [the first of Eqs. (4.2b)], respectively. However, for the corrected *bare* values none of the Cauchy relations is satisfied. Thus relatively large many body contributions are present in the *bare* values, but their effect on the Cauchy deviations is decreased by zero-point and thermal motion.

B. Comparison with theoretical-model calculation

Although a consistent calculation of the TOE constants which accounts for the Cauchy deviations obviously must include many-body interactions, it is of interest to determine whether a model with central forces only can be used to extract any information on the TOE constants from nonlinear elastic data under hydrostatic pressure, e.g., whether some TOE constants are affected by many-body contributions more than others. For this purpose we have used an anharmonic shell model to calculate the *bare* TOE constants from the *bare* values of the second-order elastic constants and of the partial contractions of the TOE constants,[4] using the equations for $c_{\mu\nu}$, $\gamma^{(3)}_{\mu\nu}$, and $c_{\mu\nu\lambda}$ given in Refs. 25, 4, and 3, respectively.[26]

The model is a natural extension of the harmonic rigid-shell model of Cowley[25] for cubic perovskites (composition ABX_3) in which pair potentials $\varphi_\alpha(r_\alpha)$ are assumed to describe the short-range interactions between nearest-neighbor ions, with $\alpha=1,2,3$ denoting the *A-X*, *B-X*, and *X-X* interactions, respectively. In this model the expressions for the second- and higher-order elastic constants are additively composed of the Coulomb and short-range interactions.[3,4,25] The former depend only on the ionic charges Z_i (for which we have used the free-ion values[27] $+1,+2,-1$ for $i=A,B,X$, respectively), but not on the ionic polarizability of the ions. In this case the anharmonic shell model contains as empirical parameters the first, second, and third derivatives of the pair potentials, which in the usual dimensionless form[3,4,25] are denoted by B_α, A_α, and C_α, respectively. However, since the second- (and third-)order elastic constants depend on the *A-X* and *X-X* interactions only in the additive form[3,25] $B_{13}=B_1+B_3$ and $A_{13}=A_1+A_3$ (and $C_{13}=C_1+C_3$), there are only four independent harmonic parameters B_{13}, B_2, A_{13}, and A_2, and two independent anharmonic parameters C_{13} and C_2. The harmonic parameters were determined from the *bare* values of the second-order elastic constants, and the anharmonic parameters from the *bare* values of the partial contractions $\gamma^{(3)}_{\mu\nu}$ of the TOE constants from Ref. 4.

Since the present model includes only central forces, the theoretical expressions satisfy the Cauchy relations (4.1) for the *bare* values of the second-order elastic constants, of the TOE constants, and of the partial contractions of the TOE constants, viz.,

$$\gamma^{(3)}_{12}=\gamma^{(3)}_{44}\ . \tag{4.3}$$

Thus there are only two theoretical expressions each available for the determination of the four harmonic and the two anharmonic parameters, viz., $c_{11},c_{12}=c_{44}$ and $\gamma^{(3)}_{11},\gamma^{(3)}_{12}=\gamma^{(3)}_{44}$, respectively. One more condition for the harmonic parameters is given by the equilibrium condition.[3,4,25] For $KMnF_3$ we have determined the parameter B_{13} from the Huggins-Mayer form, viz., $\varphi_\alpha(r_\alpha)=b_\alpha\exp(-r_\alpha/\rho)$ for $\alpha=1,3$, with b_α and ρ for the K-F and F-F interactions taken as the values determined for alkali halides,[28] resulting in a value[29] of $B_{13}=-1.2407$.

Since it is not known *a priori* which of the elastic constants in Eqs. (4.1)–(4.3) is responsible for the observed Cauchy deviations, in the empirical determination of the

parameters one has the choice between using either (i) c_{12} and $\gamma_{12}^{(3)}$, or (ii) c_{44} and $\gamma_{44}^{(3)}$ as input data. The TOE constants calculated from option (i) [(ii)] are (in 10^{10} N/m^2) $c_{111}=-50.2$ [-157.4] and $c_{122}=-43.5$ [-17.1], respectively. In the present model c_{123} depends only on the Coulomb interaction which for $KMnF_3$ has the value -5.97×10^{10} N/m^2. Only the value for c_{112} from option (ii) agrees within the estimated experimental error with the recommended *bare* value in Table IV. The arithmetic averages from options (i) and (ii) agree somewhat better (within 17 and 43 % for c_{111} and c_{112}, respectively) with the recommended *bare* values. Therefore, we have entered these average values from options (i) and (ii) for all second- and third-order elastic constants for comparison with the recommended extrapolated experimental values in Table IV. One may conclude from this comparison that the second-, and especially all third-order elastic constants are affected significantly by many-body contributions. More specifically, it is apparent that c_{166} is more strongly affected than c_{112}, and c_{144} and c_{456} are more strongly affected than c_{123}.

Although for $KMnF_3$ the average from options (i) and (ii) does roughly account for the TOE constants c_{111} and c_{112}, it is more than doubtful that this procedure may be used in general to obtain theoretical estimates when experimental data are lacking. Thus, at least for $KMnF_3$, adequate theoretical treatments of anharmonic properties must include many-body contributions,[30] either in the form of empirical potentials or through first-principle calculations.

C. Comparison of TOE constants for some perovskite compounds

Having determined the third-order elastic constants for $KMnF_3$, it is instructive to compare these data with those available for other perovskite compounds. Table V lists the room-temperature values of TOE constants for five different perovskite materials together with their lattice constants. With the exception of the data for $RbMnF_3$ (which were determined from sound-velocity measurements in hydrostatically and uniaxially stressed crystals) they were measured by means of SHG and represent uncorrected data.

It appears that, with the exception of c_{111}, no clear pattern can be discerned from the data of Table V. For ionic crystals the theoretical expressions for the third-order elastic constants contain a factor e^2/r^4, where e is the electrical charge of the ion and r the interionic distance.[23] Therefore, the magnitude of these elastic constants should decrease with increasing lattice constant and increase with the ionic charge. This is roughly the case for c_{111}; for the four fluoroperovskites the values of c_{111} are of the same order of magnitude and are roughly one fourth of the value for $SrTiO_3$; this is in accord with theoretical expectation because the charge of the oxygen ion is twice that of the fluorine ion. The dependence on lattice constant does not hold; this suggests that the contribution from the repulsive forces is large. This is even more pronounced for the other constants for which the data do not show any regular pattern.

The Cauchy relations for the TOE constants are poorly satisfied for the perovskites, which indicates large contributions from many-body forces. This suggests that every material must be considered separately.

V. SUMMARY AND CONCLUSIONS

We have measured the elastic nonlinearity parameters K_3 (defined in Table I) of $KMnF_3$ along [100], [110], and [111] by means of acoustic SHG from room temperature to 348 K. By combining these results with our earlier data[4] on the temperature dependence of the pressure derivatives of the second-order elastic constants we have determined all six TOE constants in this temperature range. The salient features of the results and their analysis are the following.

(i) Above 320 K within the scatter of the experimental data $K_3^{[100]}$ and $K_3^{[110]}$ depend linearly on temperature; below about 325 K $K_3^{[111]}$ shows modulated behavior which is within the scatter of the data compatible with linear behavior above this temperature (Fig. 5).

(ii) Above room temperature the TOE constants c_{111}, c_{123}, and c_{166} show linear temperature dependence; c_{112} and c_{144} show small upward and downward curvature, respectively; and c_{456} shows small conspicuous modulations resulting from the corresponding behavior of $K_3^{[111]}$ (Fig. 6).

(iii) After applying the Lommel diffraction correction to the nonlinearity parameters these quantities and the partial contractions of TOE constants from hydrostatic pressure measurements were extrapolated linearly from

TABLE V. Comparison of third-order elastic constants for some perovskite compounds at room temperature (in 10^{10} N/m^2).

	$SrTiO_3$	$KZnF_3$	$KMnF_3$	$RbMnF_3$	$CsCdF_3$
Ref.	31	16	present	32	16
a (Å)	3.905	4.055	4.19	4.25	4.465
c_{111}	-496 ± 43	-166	-137	-184	-132
c_{112}	-77 ± 16	-47.5	-2.5	-24	-45.5
c_{166}	-30 ± 12	-17.9	-14	-18	-6.9
c_{123}	2 ± 43	32	-44	4	26
c_{144}	-81 ± 24	-5.2	1.2	-6	-31.2
c_{456}	9 ± 27	-68.7	-2.1	-5	-38

above about 320 K to absolute zero. The static values so obtained represent *bare* TOE constants, i.e., without the effects of zero-point and thermal motion, and without the effect from the improper ferroelastic phase transition of 186 K.

(iv) The *bare* TOE constant data are subject to errors from some uncertainties in the diffraction correction, from other conceivable systematic errors of the SHG technique, and from the relatively low maximum temperature accessible with the available SHG equipment, which prevented us from verifying that the regime of a strictly linear temperature dependence had been reached for all TOE constants.

(v) Both the *bare* and the room temperature values of the TOE constants show large deviations from the Cauchy relations, indicating large many-body contributions to the interatomic forces (Table IV).

(vi) As expected from (v) the *bare* TOE constants could not be calculated satisfactorily from the *bare* values of the pressure coefficients of the second-order elastic constants by using an anharmonic rigid-shell model with Coulomb-plus-central-force interactions between the three types of nearest-neighbor interactions (Table IV).

(vii) An adequate theoretical treatment of anharmonic properties in $KMnF_3$ must include many-body interactions which can be fitted to, or must reproduce the *bare* TOE constants presented here. Work in this direction is already in progress.

ACKNOWLEDGMENTS

It is a pleasure to acknowledge ongoing discussions with Dr. B. N. N. Achar and Dr. L. E. Cross on perovskites in general. This work was supported by the U.S. Office of Naval Research under Contract No. N00014-82-K-0339.

---

†Present address: National Center for Acoustics, P.O. Box 847, University, Mississippi 36877.

*Permanent address: Nanjing University, The People's Republic of China.

[1]O. Muller and R. Roy, *The Major Ternary Structural Families* (Springer, Berlin, 1974), p. 175.

[2]M. E. Lines and A. M. Glass, *Principles and Applications of Ferroelectrics and Related Materials* (Clarendon, Oxford, 1977).

[3]B. N. N. Achar, G. R. Barsch, and L. E. Cross, Phys. Rev. B **24**, 1209 (1981).

[4]W. Cao and G. R. Barsch, Phys. Rev. B **38**, 7947 (1988); W. Cao, Ph.D. Thesis, The Pennsylvania State University (1987).

[5]M. A. Breazeale and J. Philip, in *Physical Acoustics*, edited by W. P. Mason and R. N. Thurston (Academic, New York, 1984), Vol. XVII, pp. 1–60.

[6]Z. A. Goldberg, Akust. Zh. **6**, 307 (1960) [Sov. Phys.—Acoust. **6**, 306 (1961)].

[7]M. A. Breazeale and J. Ford, J. Appl. Phys. **36**, 3486 (1965).

[8]R. E. Green, Jr., in *Treastise on Materials Science and Technology*, edited by H. Herman (Academic, New York, 1973), Vol. 3, p. 1.

[9]W. B. Gauster and M. A. Breazeale, Rev. Sci. Instrum. **37**, 1544 (1966).

[10]E. Lommel, Abh. Bayer. Akad. Wiss. Math.-Naturwiss. Kl. **15**, 233 (1886); see also A. Gray, G. B. Mathers, and T. M. Mac Robert, *A Treatise on Bessel Functions* (MacMillan, London, 1931), Chap. 14.

[11]P. H. Rogers and A. L. Van Buren, J. Acoust. Soc. Am. **55**, 724 (1974).

[12]B. D. Blackburn and M. A. Breazeale, J. Acoust. Soc. Am. **76**, 1755 (1984).

[13]In this case the discrepancy between the SHG data for Cu by Blackburn and Breazeale (Ref. 12) and those of Gauster and Breazeale [Phys. Rev. **168**, 655 (1968)] would increase. In addition, if the statement (Ref. 12) "that a diffraction correction (for the data of Gauster and Breazeale) was not considered necessary" were retracted and the diffraction correction is actually applied to $K_S^{[111]}$ the discrepancy between these two sets of data would increase further. Perhaps this could be attributed to sample differences and other systematic errors, as discussed in the text.

[14]A series expansion for the Lommel diffraction integral has been given by A. O. Williams [J. Acoust. Soc. Am. **48**, 286 (1970)]; however, the derivation contains inconsistencies and we have been unable to reproduce his result.

[15]H. Sakashita and N. Omaha, Phase Transitions **2**, 263 (1982).

[16]M. A. Breazeale, J. Philip, A. Zarembovich, M. Fischer, and Y. Gesland, J. Sound Vib. **88**, 133 (1983).

[17]R. Truell, C. Elbaum, and B. B. Chick, *Ultrasonic Methods in Solid State Physics* (Academic, New York, 1969), p. 190.

[18]E. L. Meeks and R. T. Arnold, Phys. Rev. B **1**, 982 (1970).

[19]E. Pytte, in *Structural Phase Transitions and Soft Modes*, edited by E. J. Samuelsen, E. Anderson, and J. Feder (Universitetsforlaget, Oslo, 1971).

[20]U. T. Höchli and A. D. Bruce, J. Phys. C **13**, 1963 (1980).

[21]H. Hahn, in *Inelastic Scattering of Slow Neutrons from Solids and Liquids* (IAEA, Vienna, 1963), Vol. 1, p. 37.

[22]G. Leibfried and W. Ludwig, in *Solid State Physics*, edited by F. Seitz and D. Turnbull (Academic, New York, 1961), Vol. 12, p. 275.

[23]P. B. Ghate, Phys. Rev. **139**, 1666 (1965).

[24]G. R. Barsch, Phys. Status Solidi **19**, 129 (1967).

[25]R. A. Cowley, Phys. Rev. **134**, A981 (1964).

[26]The entries for Table VI of Ref. 3 for the off-diagonal elements of the Coulomb sums $\gamma_{\mu\nu\lambda}^{\alpha\beta}$ as defined by Eq. (A2) contain a redundant factor of 2, i.e., the actual values are for $\alpha \neq \beta$ equal to half the values given there. Likewise, the Madelung constant α_M as given by Eq. (A6) contains a redundant factor of 2 when the Coulomb energy per unit cell is defined (as usual) as $\alpha_M e^2/a$, where a is the lattice constant. Note that in this definition the negative sign of the Coulomb energy is absorbed in the definition of α_M, consistent with the sign of the Coulomb contribution to the equilibrium condition, Eq. (A5) of Ref. 3. All numerical results in Ref. 3 were obtained by using the correct equations.

[27]When the effective ionic charges and the other shell model parameters are fitted both to elastic constants and phonon-dispersion data significantly different values than these free-ion values can be obtained. Since cohesive energies of ionic

crystals are generally accounted for best with free-ion charges it seems more plausible, however, to use these values for elastic constant calculations, unless deformation-induced charge-transfer effects are included which go beyond the rigid-shell model.

[28]M. P. Tosi, in *Solid State Physics,* edited by F. Seitz and D. Turnbull (Academic, New York, 1964), Vol. 16, p. 1, Table IX. Since our analysis is intended to be only approximate we neglect the van der Waals contributions included in the Huggins-Mayer treatment.

[29]Since the second (and third) derivatives A_α, (C_α) are roughly ten (hundred) times larger than the first derivatives B_α, respectively, this introduces only a small error in the result.

[30]S. K. Singh, Phys. Rep. **85**, 259 (1982).

[31]A. G. Beattie and G. A. Samara, J. Appl. Phys. **42**, 2376 (1971).

[32]E. R. Naimon and A. V. Granato, Phys. Rev. B **7**, 2091 (1973).